

Topical Review

Review on polymer-stabilized short-pitch cholesteric liquid crystal displays

Guanjun Tan¹, Yun-Han Lee¹, Fangwang Gou¹, Haiwei Chen¹, Yuge Huang¹, Yi-Fen Lan², Cheng-Yeh Tsai² and Shin-Tson Wu¹ 

¹ College of Optics and Photonics, University of Central Florida, Orlando, FL 32816, United States of America

² Advanced Display Technology Centre, AU Optronics Corp., Hsinchu 30078, Taiwan

E-mail: swu@ucf.edu

Received 14 August 2017, revised 20 September 2017

Accepted for publication 5 October 2017

Published 2 November 2017



CrossMark

Abstract

Submillisecond response times and low operation voltage are critical to next generation liquid crystal display and photonic devices. In this paper, we review the recent progress of three fast-response short-pitch cholesteric liquid crystal modes: blue phase (BP), uniform standing helix (USH), and uniform lying helix (ULH). This review starts with a brief introduction of device structures and working principles, and then highlights two competing electro-optical effects: dielectric effect and flexoelectric effect. Next, we compare their electro-optical behaviors, response time, temperature dependence, and contrast ratio. Based on our established simulation model, we are able to optimize the phase compensation scheme for improving the viewing angle and gamma shift of USH and ULH modes. Finally, we analyze some major challenges, which remain to be overcome before the widespread applications of these liquid crystal devices can be realized.

Keywords: liquid crystals, flexoelectric effect, cholesteric liquid crystals, fast switching time

(Some figures may appear in colour only in the online journal)

1. Introduction

After nearly half a century of material innovation, extensive device development, and heavy investment on advanced manufacturing technologies, thin-film-transistor (TFT) liquid-crystal displays (LCDs) [1] have become ubiquitous in our daily lives. Their widespread applications cover from smartphones, tablets, computer monitors, to large-screen TVs. Lately, organic light emitting diode (OLED) display [2] is arising and its applications focus on smartphones and TVs. ‘LCD versus OLED: who wins?’ is a hot debate topic [3–5]. Generally, LCD shows advantages in long lifetime, peak brightness, and low cost; while OLED performs better in dark state, flexibility, and response time. To face the challenges from OLED, LCD camp keeps developing new technologies. For examples, local dimming helps boost the

LCD dynamic contrast ratio (CR) to 1000000:1 [6, 7], and quantum-dot enhanced LCDs provide even wider color gamut than OLEDs [8–10]. Lately, transparent LCD with 80% transparency [11] and rollable LCD with organic TFTs [12] are emerging. While in terms of image blurs, LCD suffers about 100× slower response time than OLED, which thus becomes the main challenge for LCDs. By considering the TFT sample-and-hold addressing mechanisms, object motion, and human vision system, the concept of motion picture response time (MPRT) is proposed as a more comprehensive metric to evaluate the image blurs of active matrix displays, including both LCDs and OLEDs. Recent analyses indicate that, at the same frame rate, e.g. 120 Hz, if the LC response time is below 2 ms, then its MPRT is comparable to that of OLED [13]. In addition to the intrinsic LC (or OLED) response time, two other factors also affecting the MPRT are frame rate and duty

ratio. Another motivation for fast response time is to enable field-sequential color (FSC) displays. By removing the spatial color filters, both optical efficiency and resolution density can be tripled. However, in order to suppress crosstalk and color breakup for FSC displays [14], the LC response time should be less than 1 ms [15]. Moreover, with the recent rapid growth of wearable near-eye displays, like virtual reality (VR) and augmented reality (AR), there is also urgent need on fast MPRT to reduce latency [16].

The gray-to-gray (GTG) response time of a nematic LC device is governed by the visco-elastic constant of the employed LC material, cell gap, and applied voltage [17]. A typical LCD's response time is around 5–10 ms. To achieve a faster response time, several approaches have been proposed, including ultra-low viscosity LC material [18, 19], thin cell gap [20], overdrive and undershoot driving scheme [21], and triode configurations [22–25]. Each approach has its own pros and cons. In addition to nematic, ferroelectric liquid crystal (FLC) also attracts a lot of research interest due to its sub-millisecond response time, low operation voltage, and wide viewing angle. However, its CR, mechanical and shock stabilities, and geometrical defects remain to be improved. Recently, with the development of new operation modes [26] and photo-alignment materials [27], FLC is becoming a promising technology for FSC displays. Meanwhile, some short-pitch cholesteric liquid crystals (CLCs) have also been actively explored, such as polymer-stabilized blue phase liquid crystal (BPLC) [28–30], chiral nanostructured LC [31], and polymer-stabilized hyper-twisted nematic (HTN) liquid crystals [32–38]. All these short-pitch CLC modes can offer submillisecond response time, but the tradeoff is relatively high operation voltage. One thing worth mentioning is that for display applications, the pitch length of these modes is usually short so that their associated Bragg reflections occur in the UV region. The display panel appears clear in the visible region.

Blue phase (BP) got its name because the Bragg reflection just happened to appear in the blue region when the first BP compound was discovered. BP exists between chiral nematic and isotropic phases. At the beginning stage, the development of BP was limited by its narrow (1–2 °C) temperature range. In 2002, Kikuchi *et al* successfully extended the BP temperature range to over 60 °C by adopting polymer stabilization [29]. From then on, polymer-stabilized blue-phase liquid crystal (PS-BPLC) opens a new gateway for next generation display and photonics applications [39–42]. PS-BPLCs exhibit several unique features, for instance self-assembly structure, high CR [43], wide viewing angle and submillisecond response time [44, 45], which are highly favorable for display applications. Although PS-BPLC is potentially a strong candidate for next generation displays, its relatively high operation voltage and slow capacitance charging time need further improvement. Recently, with newly developed materials [15, 45, 46], optimized protrusion electrodes [47–51], and bootstrapping driving scheme [50–53], AU Optronics has demonstrated a 12" FSC BP LCD prototype [51].

In parallel, the polymer-stabilized HTN liquid crystals also attract a great deal of attention. Two types of HTN

configurations exist, namely uniform lying helix (ULH) [33–35] and uniform standing helix (USH) [36–38]. The helical axis in ULH mode is uniformly aligned to be parallel to the substrate surface, and the LC directors are reoriented by the longitudinal electric fields. In contrast, the helical axis of USH is perpendicular to the substrate surface and it takes fringing electric fields to reorient the CLC. Therefore, to realize the useful EO effects of an USH cell, in-plane switching (IPS) electrodes should be used [36–38]. Both ULH and USH modes can provide submillisecond response time due to their subwavelength pitch length. In HTN modes, dielectric effect and flexoelectric effect often coexist [35]. For low power display applications, the on-state voltage should be lower than 15 V. As a result, LC materials with a large flexoelectric effect are preferred. Lately, bimesogenic [54–57] and bent-core [58] compounds are found to exhibit a relatively large flexoelastic coefficient. In particular, new LC materials with a giant flexoelastic coefficient [59, 60] have been developed, which helps reduce the operation voltage to ~15 V. Thus, HTN modes take a further step toward practical applications.

The major objective of this review paper is to analyze and compare the performances of three short-pitch CLC modes, BPLC, USH and ULH, for display and photonic applications. In section 2, we describe the device structures and basic working principles. We also introduce the sample preparation procedures of these three modes, especially the ULH alignment. Two key EO effects (dielectric and flexoelectric) and their respective roles are analyzed. In section 3, from the application viewpoint we analyze the EO behaviors of these three modes including simulation models, voltage-dependent transmittance (VT) curves, response time, and temperature dependence. In section 4, we investigate the CR and viewing angle properties, and then propose some compensation methods for the multi-domain structures. In section 5, we discuss the major challenges of these LC modes when facing practical applications.

2. Basic working mechanism

2.1. Device structure

Figures 1(a)–(f) depict the device configurations and the LC director distributions of these three short-pitch CLC modes. BP possesses self-assembled structure. Depending on the lattice structures, BPLCs can have three structures: BPI (figure 1(b)), BPII (figure 1(c)) and BPIII. Both BPI and BPII consist of double-twist cylinders. Figure 1(d) visualizes the local director field of the double-twist cylinder. The central LC director is along the helical direction of the cylinder, while from center to surface the LC director twists continuously along the radial direction (figure 1(d)). BPI exhibits a body-centered cubic structure (figure 1(b)), BPII has a simple cubic structure (figure 1(c)) [40], while BPIII has an amorphous structure [61]. Overall, the helical axis of the cholesteric LCs in BPs can be in any direction, as figures 1(b)–(d) indicate. Therefore, BPLC is optically isotropic in the voltage-off state, assuming its Bragg reflection is in the UV region. Both lateral field and longitudinal field can be used to generate effective birefringence. To

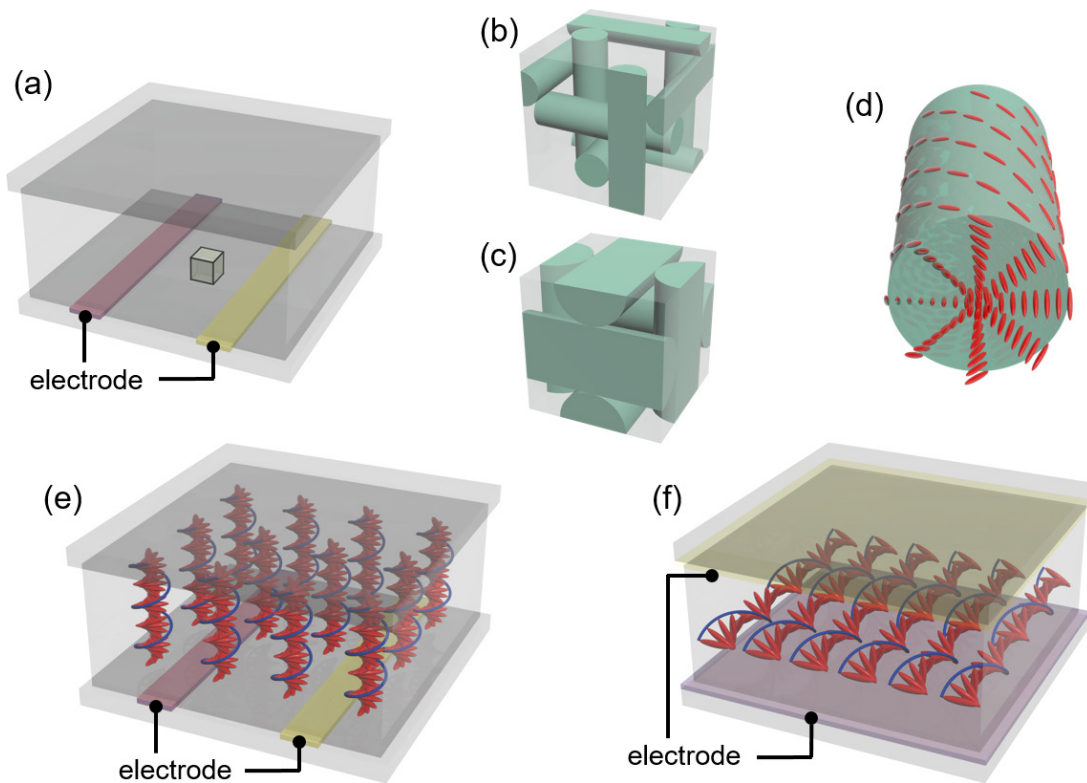


Figure 1. Structure scheme of BP LC, USH and ULH devices. (a) BP LC in an IPS cell, (b) lattice structure of BPI, (c) lattice structure of BPII, (d) BPLC directors distribution in the double-twist cylinder, (e) USH device in an IPS cell, and (f) ULH device in a homogenous cell.

generate lateral field, an IPS cell with interdigitated pixel electrodes is commonly employed, as figure 1(a) shows. To utilize longitudinal field, another device scheme called vertical field switching (VFS) [62, 63], which offers a much lower voltage, higher transmittance, and negligible hysteresis in comparison with the IPS mode. However, VFS requires a complicated optical system, such as oblique directional backlight and special phase compensation, to achieve a wide view [64]. These drawbacks limit the applications of VFS mode for displays. Here, we will focus on the IPS-based BPLC.

As for the HTN cells, the helical axis of cholesteric LC pitch is aligned uniformly. USH and ULH modes bear their names according to the CLC helix alignment directions. The LC director distribution in a USH cell is similar to that of a planar cholesteric LC, whose helical axis is perpendicular to the substrate surface (figure 1(e)). To reorient the LC directors in such a USH cell, IPS electrodes are commonly utilized. While in a ULH cell, the helix is unidirectionally aligned parallel to the substrate surface (figure 1(f)). In the voltage-on state, the top and bottom planar electrodes generate longitudinal fields to reorient the helical axis of the CLC. Correspondingly, the optical axis in an ULH cell shows unique uniform in-plane switching [33, 34].

2.2. Sample preparation

Before measuring the EO properties, we need to formulate LC mixtures and fabricate the test cells. The typical sample preparation procedures of BPLC, USH and ULH cells are briefly described as follows.

A PS-BPLC precursor consists of 70–90 wt.% nematic LC host as switching molecules, 5–10 wt.% chiral dopant to induce BP, and 8–15 wt.% photo-curable monomers and 1 wt.% photo initiator for polymer stabilization [41, 65]. After mixture formulation, we injected the LC mixture into an IPS cell at an isotropic state, and then cooled down the sample slowly to BP, observed under a polarizing optical microscope. Once the BP appeared, we exposed the cell with UV light to form a polymer-stabilized BPLC composite. The material systems and polymerization processes of PS-BPLCs have been discussed extensively [40, 41, 65, 66]. Since the formation of PS-BPLC involves a self-assembly process, additional surface alignment layer is not necessary. The alignment layer may help to form uniform BP lattice [67] while it also results in voltage shielding effect [68]. For display applications, it is important to shift the Bragg reflection to the UV region. This can be done easily by controlling the concentration and the helical twisting power (HTP) of the chiral dopant.

Until now, most of reported USH devices mainly utilize dielectric effect [37, 38]. Therefore, these USH precursors are quite similar to PS-BPLC [37, 38, 69–71]. However, there is another important EO effect called flexoelectric effect in a HTN cell. Some bimesogenic [54–57, 60] and bent-core [58] LC materials with strong flexoelectric effect can be doped into USH precursors as well [71, 72]. We injected the USH precursors into an IPS cell, as figure 1(e) illustrates. During sample preparation, we gradually cooled the USH LC cell from an isotropic phase to room temperature to obtain uniformly aligned CLC texture. Next, we cured the cell by UV light to stabilize the uniform texture for repeated driving.

Table 1. Typical alignment methods to get uniform ULH pattern.

Alignment method	Anchoring condition	Electrical treatment	Thermal treatment	Mechanical treatment	CR
Cooling	HG alignment [33, 34]	AC	Cool from Iso	No	—
	TN alignment [73]	AC	Cool from Iso	No	~650:1 (laser)
Shearing force [74–76]	No alignment	AC	No	Oscillatory shear	—
Periodic anchoring	Groove by interference exposure [78]	No	No	No	>100:1 (white light)
	Groove by laser writing [80]	AC	Cool from Iso	No	—
	Groove by molding [82]	No	Cool from Iso	No	—
	Periodic HG/HT alignment [77]	AC	Cool from Iso	No	—
	Cholesteric alignment [79]	AC	Cool from Iso	No	—
Electro-hydrodynamic induction [83, 84]	Scratched surface [81]	No	Cool from Iso	No	—
	HG alignment	AC	No	No	—
BP-ULH transition [35, 84]	HG alignment	AC	At BP state	No	~240:1 (laser)
Tri-electrode [87]	HG alignment	AC	No	No	~50:1

Note: HG: homogenous; TN: twisted-nematic; Iso: isotropic; HT: homeotropic.

A large flexoelectric effect helps reduce the operation voltage of an ULH cell. Therefore, ULH precursors usually consist of a relatively high concentration of bimesogenic compound [35, 54–57, 60] or bent-core structure [58] to provide strong flexoelectric effect. Unlike BPLC and USH modes, ULH mode needs special treatment to obtain uniform alignment pattern. A variety of methods involving combinations of electrical, mechanical or thermal treatment [70–73], periodic anchoring [77–82], electro-hydrodynamic effects [83, 84], BP-ULH transition [38, 85, 86], tri-electrodes configuration [87] and slit coater [88] have been proposed. In table 1, we list several alignment approaches to obtain uniform ULH pattern. How to achieve uniform alignment remains a big challenge. Up to now, ULH mode still suffers from complicated alignment procedures and relatively low CR. In order to achieve long-term stability of the ULH texture, bulk or surface localized polymer network [74, 89–91] can be employed. The parameter optimization of polymerization process for ULH mode, including polymer concentration and curing temperature, has been investigated in [89].

2.3. Working principles

For display applications, the LC cell, which provides effective phase retardation, is sandwiched between two crossed polarizers, and the whole panel works as a spatial light intensity modulator. Unlike nematics, the short-pitch CLCs can be macroscopically treated as an effective homogenous medium [92] when the pitch length is much shorter than the wavelength. Under such condition, the macroscopic description of EO behaviors is adequate for the short-pitch CLC modes.

The working mechanisms of these three modes are based on two electro-optical effects: dielectric effect and flexoelectric effect. The LC director reorientations within single pitch under these two effects are simulated and results plotted in figure 2. The LC director distributions are calculated by minimizing the free energy with fixed boundary condition [35]. The LC director profile provides useful information for us to

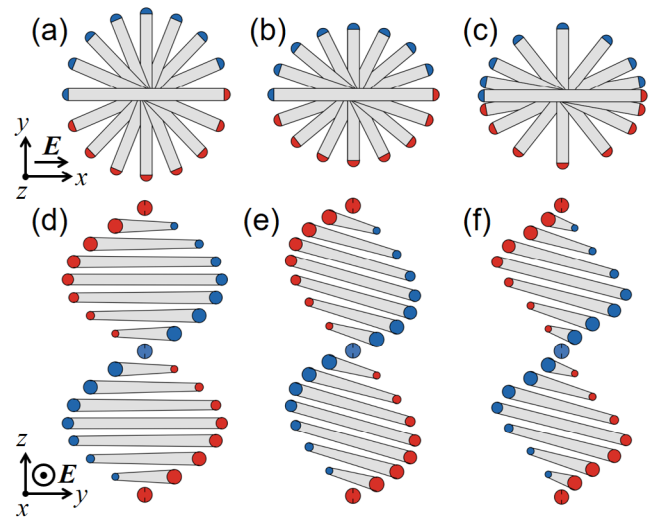


Figure 2. Schematic LC director distribution. (a), (d) Without applied electric field; (b), (e) under pure flexoelectric effect with applied electric field; and (c), (f) under dielectric effect and flexoelectric effect with applied electric field.

understand the macroscopic EO performance. The helix axis of CLC is along the z direction, and the applied electric field is along the x direction. At the initial state without voltage (figures 2(a) and (d)), the LC directors are twisted along helix axis, same as conventional CLCs. When the electric field is applied perpendicular to helix axis, pure flexoelectric effect makes the LC directors to tilt uniformly (figures 2(b) and (e)). When both flexoelectric effect and dielectric effect are present, the latter causes some distortion to the uniform tilt (figure 2(f)). As a result, the LC directors are pulled toward the electric field direction because of the exerted dielectric force (figure 2(c)). The LC director distribution essentially determines the macroscopic optical performance.

The EO effect of BPLC is mainly governed by the dielectric effect, known as Kerr effect. At the voltage-off state, the helical axis of CLC in a BP can be in any direction (figure 1(d)), which makes BPLC optically isotropic. As

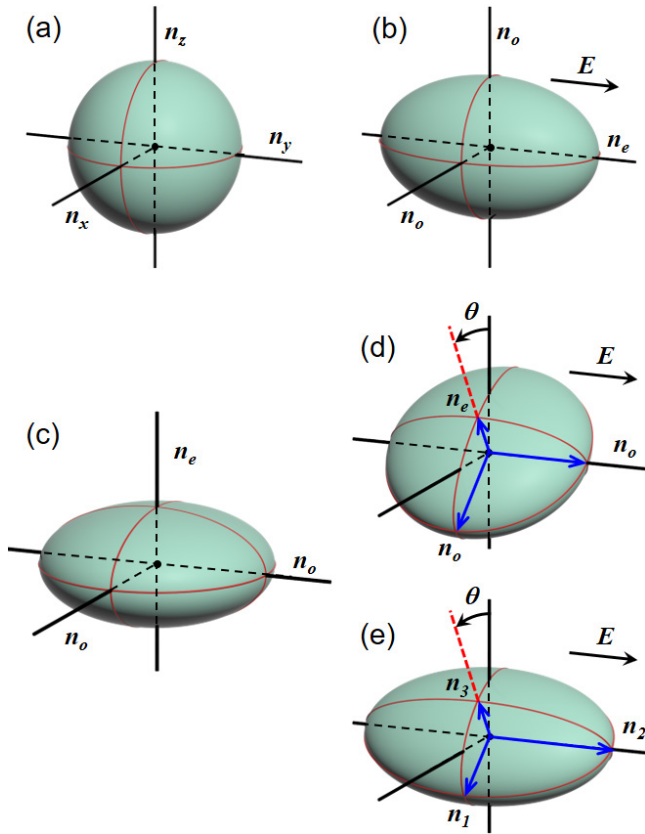


Figure 3. Macroscopic refractive index ellipsoids of BPLC and HTN modes. BPLC mode: (a) without and (b) with applied electric field. HTN modes: (c) without applied electric field; (d) under pure flexoelectric effect with applied electric field; and (e) under dielectric effect and flexoelectric effect with applied electric field.

the voltage increases, the electric field-induced isotropic-to-anisotropic transition takes place. The macroscopic electro-optical response of BPLC are presented in figures 3(a) and (b). The electric field elongates the refractive index ellipsoid. For a BPLC material with positive dielectric anisotropy, n_e is larger than n_o . The BPLC transitions from isotropic medium to *uniaxial* medium under an electric field.

While for HTN modes, the initial state is macroscopically uniaxial, considering the sub-wavelength pitch length. Figure 3(c) illustrates the initial refractive index ellipsoid, which is corresponding to the LC director distribution in figures 2(a) and (b). The optic axis is parallel to the helical axis of CLCs. The extraordinary refractive index is smaller than the ordinary refractive index, like a negative C film. When only flexoelectric effect is present, the flattened ellipsoid rotates around the electric field direction, while keeping the principal refractive indices unchanged (figure 3(d)). Sometimes, flexoelectric effect and dielectric effect exist simultaneously in a HTN mode. In this case, the LC directors are depicted in figures 2(c) and (f). The respective roles of these two effects can be distinguished easily as follows: flexoelectric effect rotates the refractive index ellipsoid around the electric field direction (figure 3(e)), while dielectric effect helps elongate the ellipsoid along the electric field direction, as depicted in figure 3(e). The principal refractive index n_2 (parallel to electric field) increases as electric field increases, but n_1

(perpendicular to electric field) decreases. Both flexoelectric effect and dielectric effect contribute to the effective birefringence change. The final ellipsoid becomes *biaxial*, which is different from BPLC.

3. Electro-optical behaviors

3.1. Simulation model

To simulate the electro-optical behaviors of a nematic LC device, we first calculate the LC director distribution at a given voltage and then its corresponding optical properties. For the above-mentioned three short-pitch CLCs, their EO simulation follows similar steps as well; the only difference is that the optical modelling of short-pitch CLCs is based on the macroscopic optical behaviors.

For BPLCs, extensive simulation efforts have been devoted to. The dielectric effect, or Kerr effect, is a quadratic EO effect. The electric field-induced refractive index ellipsoid is uniaxial, as illustrated in figure 3(b). In the weak field region, the induced birefringence can be described by Kerr effect as:

$$\Delta n_{\text{ind}} = \lambda K E^2, \quad (1)$$

where λ is the wavelength, E is the electric field, and K is the Kerr constant. Kerr constant is a key parameter affecting the EO performance of BPLCs. From Gerber's model [28], Kerr constant is governed by the intrinsic LC birefringence (Δn), dielectric anisotropy ($\Delta \epsilon$), average elastic constant (k), and pitch length (p) of the chiral LC host as [28]:

$$K = \Delta n \Delta \epsilon \frac{p^2}{\lambda k (2\pi)^2}. \quad (2)$$

Considering practical device configurations, Ge *et al* proposed a simulation model, which directly relates the macroscopic refractive index with local electric field vector [39]. The distribution of electric field \mathbf{E} in the device was calculated first by solving the Poisson equation, and then the induced birefringence distribution (equation (1)); the optic axis direction can be further assigned based on the local electric field. However, equation (1) is valid only in the weak electric field region. As the electric field keeps increasing, the induced birefringence will eventually saturate. Under such condition, Yan *et al* proposed following extended Kerr model [93]:

$$\Delta n_{\text{ind}} = \Delta n_{\text{sat}} \left(1 - \exp \left[- (E/E_s)^2 \right] \right), \quad (3)$$

where Δn_{sat} is the saturated refractive index change and E_s stands for the saturation electric field. The principal refractive indices n_e and n_o in figure 3(b) can be determined by the following equations [93]:

$$n_e = n_{\text{iso}} + \frac{2}{3} \Delta n_{\text{ind}}, \quad (4a)$$

$$n_o = n_{\text{iso}} - \frac{1}{3} \Delta n_{\text{ind}} \quad (4b)$$

where n_{iso} is the initial isotropic refractive index, which can be determined by the average of intrinsic ordinary and

extraordinary refractive indices of the LC composite [93]. From equations (3), (4a) and (4b), the EO response of BPLC can be simulated. Later, an improved model by considering the optical refraction effect in an IPS cell was proposed by Xu *et al* [94].

As for HTN modes, both the dielectric effect and flexoelectric effect need to be considered. In 1969, Meyer discovered the flexoelectric effect [32]. This effect can be applied to describe the coupling between electric polarization (P_f) and splay-bend elastic distortions in nematic LCs:

$$\mathbf{P}_f = e_s \hat{\mathbf{n}} (\nabla \cdot \hat{\mathbf{n}}) - e_b \hat{\mathbf{n}} \times (\nabla \times \hat{\mathbf{n}}), \quad (5)$$

where e_s and e_b stand for the splay and bend flexoelectric coefficient, respectively, and $\hat{\mathbf{n}}$ is the unit vector of LC director. Thus, the free energy density is given by:

$$f = \frac{1}{2} K_{11} (\nabla \cdot \hat{\mathbf{n}})^2 + \frac{1}{2} K_{22} (\hat{\mathbf{n}} \cdot \nabla \times \hat{\mathbf{n}} + 2\pi/p)^2 + \frac{1}{2} K_{33} (\hat{\mathbf{n}} \times \nabla \times \hat{\mathbf{n}})^2 - e_s \mathbf{E} \cdot \hat{\mathbf{n}} (\nabla \cdot \hat{\mathbf{n}}) + e_b \mathbf{E} \cdot \hat{\mathbf{n}} \times \nabla \times \hat{\mathbf{n}} - \frac{1}{2} \varepsilon_0 \Delta \varepsilon (\mathbf{E} \cdot \hat{\mathbf{n}})^2, \quad (6)$$

where K_{11} , K_{22} and K_{33} are the splay, twist, and bend elastic constants, respectively, p is the twist pitch length, \mathbf{E} is the applied electric field, $\Delta \varepsilon$ is the dielectric anisotropy of the LC material. In equation (6), the first three terms represent elastic energy, which is independent of electric field. The fourth and fifth terms are from the flexoelectric effect, corresponding to the flexoelectric polarization in equation (5). The last term is from the dielectric effect. By minimizing the free energy with Euler–Lagrange equations and fixed boundary conditions [35, 92], the LC director distribution can be numerically obtained. The simulated LC director distributions are plotted in figure 2. When flexoelectric effect dominates, the LC director tilts uniformly around the applied electric field direction. The rotation angle θ is correlated with the applied field as [95, 96]:

$$\tan \theta = \frac{p}{2\pi} \frac{e_s - e_b}{2K_{22}} E - \frac{K_{11} - 2K_{22} + K_{33}}{2K_{22}} \sin \theta. \quad (7)$$

By employing small angle approximation, equation (7) can be simplified as:

$$\tan \theta \approx \frac{p}{2\pi} \frac{e_s - e_b}{K_{11} + K_{33}} E = \frac{p}{2\pi} \frac{e_f}{K_f} E. \quad (8)$$

This simplified equation (8) is commonly used to fit experimental data. The effective e_f/K_f is known as flexoelastic coefficient.

Next, in order to correlate the LC director distribution with macroscopic optical behavior, Tan *et al* built a macroscopic model based on numerical finite element method (FEM) [35]. The unidirectionally aligned short-pitch CLCs optically works as a homogenous uniaxial medium, as shown in figure 3(c). The macroscopic refractive index n_e equals to the intrinsic ordinary refractive index, and the n_o in figure 3(c) is determined by the quadratic mean of intrinsic ordinary and extraordinary refractive indices of LC composite [35, 36]. The flexoelectric effect rotates the optic axis by an angle θ (equation (7)). At the same time, dielectric effect elongates the refractive index ellipsoid along the electric field direction. The induced birefringence can also be described by equation (3) due to same working mechanism. The principal

refractive indices of optically biaxial medium, as indicated in figure 3(e), can be determined by:

$$n_1 = n_o - \frac{1}{2} \Delta n_{\text{ind}}, \quad (9a)$$

$$n_2 = n_o + \frac{1}{2} \Delta n_{\text{ind}}. \quad (9b)$$

The n_3 in figure 3(e) keeps unchanged.

The electric field distribution in a ULH cell is uniform. Thus, the VT of a ULH cell sandwiched between two crossed polarizers is given by:

$$T = \sin^2 \left[\frac{\pi d \Delta n(E)}{\lambda} \right] \cdot \sin^2 [2\theta(E)] \quad (10)$$

where $\Delta n = n_1 - n_3$ is the effective birefringence (figure 3(e)) and θ is the rotation angle of the optic axis determined by equations (7) and (8). The first term in equation (10) describes the dielectric coupling effect, which tends to decrease the maximum transmittance and on-state voltage [35, 97]. The dependency of effective birefringence on applied electric field has been discussed exhaustively in [35].

As for USH mode, the electric field distribution is not uniform due to IPS cell configuration. We can also relate the macroscopic refractive index ellipsoid with local electric field vector [37], just like BPLCs. In previously reported simulation models for USH mode, the biaxial optical property of the macroscopic effective medium has not been considered [36–38]. Here, we propose a new model for USH mode by considering the macroscopic biaxial optical property. Unlike conventional uniaxial nematic LC or BPLC, such biaxial material possesses a different dielectric tensor. The dielectric constant tensor can be expressed as:

$$\overset{\leftrightarrow}{\varepsilon} = \begin{bmatrix} n_3^2 + (n_1^2 - n_3^2) \cos^2 \theta & 0 & (n_1^2 - n_3^2) \sin \theta \cos \theta \\ 0 & n_2^2 & 0 \\ (n_1^2 - n_3^2) \sin \theta \cos \theta & 0 & n_3^2 + (n_1^2 - n_3^2) \sin^2 \theta \end{bmatrix}. \quad (11)$$

The 3×3 dielectric constant tensor can be constructed from the local electric field. With the dielectric constant tensor distribution obtained, we can then carry out the optical simulation using 2×2 extended Jones matrix [98] or 4×4 Jones matrix [99].

Experiments have been carried out to verify our simulation model. A large $\Delta \varepsilon$ nematic LC host JC-BP01 (Merck) with pitch length ~ 182 nm was employed. The LC material was filled into an IPS test cell with cell gap ~ 8.8 μm , electrode width ~ 15 μm and electrode gap ~ 15 μm . The test cell was gradually cooled down from an isotropic state to room temperature (~ 20 $^\circ\text{C}$). Once the USH pattern was formed, we stabilized it by UV polymerization. We measured the VT curves at different wavelengths and different incident angles. The measured and simulated VT curves are plotted in figures 4 and 5, where the transmittance was normalized to the peak transmittance. The fitting parameters $\Delta n_{\text{sat}} = 0.156$, 0.148 and 0.142 for $\lambda = 457$ nm, 514 nm and 633 nm, respectively, and the saturation electric field is 6.2 $\text{V } \mu\text{m}^{-1}$, which is independent of wavelength. Excellent agreement between

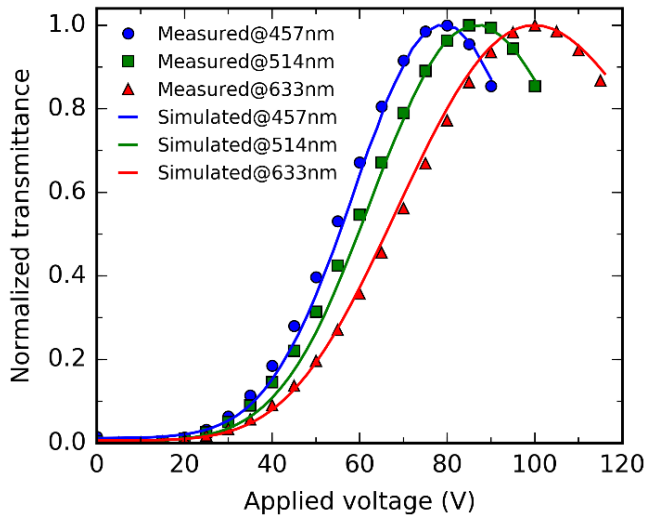


Figure 4. Measured and simulated VT curves of USH cell at $\lambda = 457$ nm, 514 nm and 633 nm.

simulated and measured results validates our proposed model. Especially, figure 5 indicates that our model can successfully predict the EO performance of USH mode, even for off-axis incident angles. That means our model can be used for viewing angle simulation. One may notice that there is a small discrepancy in figure 5. This can be accounted for by the optical diffraction of the employed IPS electrodes and the light refraction at the edges of interdigitated pixel electrodes.

3.2. Operation voltage

Operation voltage and optical transmittance are key parameters for LCDs. Low operation voltage and high optical transmittance mean low power consumption, which is especially critical for mobile devices. The operation voltage of a nematic LCD is usually in the range of 5–7 V.

The development strategy of BPLCs in recent years indeed focuses on lowering operation voltage while keeping high transmittance. To achieve this target, both LC material and device configuration need to be taken into consideration. From LC material perspective, a large Kerr constant is highly favorable for lower voltage [45, 46, 100], as equation (1) indicates. In order to enhance Kerr constant of BPLC, high birefringence and large dielectric anisotropy are preferred (equation (2)). Several large Kerr constant BPLCs with $\Delta n > 0.18$ and $\Delta\epsilon > 100$ have been developed [101, 102]. Chen *et al* reported a BPLC mixture with $K \sim 33.1$ nm V⁻² by employing a large $\Delta\epsilon$ nematic LC host JC-BP06N [45]. However, there are several concerns for such a huge $\Delta\epsilon$ BPLC material. The rotational viscosity of the LC material increases, which leads to a slower response time (>1 ms). In addition, high $\Delta\epsilon$ would result in longer capacitor charging time for TFT addressing [15]. The charging issue can be overcome by special driving circuit design, for instance bootstrapping driving method [52, 53]. On the other hand, optimizing device structure can also reduce operation voltage, such as protrusion electrodes [47–51], corrugated electrodes [103] and double-penetrating fringe fields [104]. Recently, an optimized BP LCD with LC

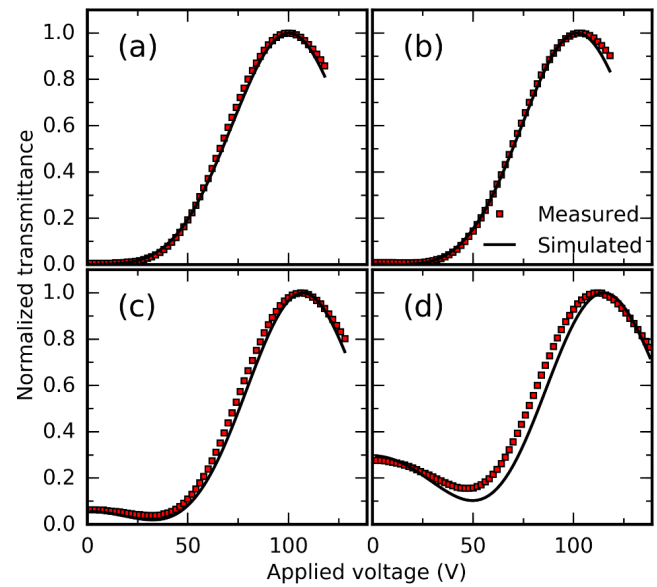


Figure 5. Measured and simulated VT curves of USH cell at 633 nm with different incident angles: (a) 0°; (b) 10°; (c) 20° and (d) 30°.

mixture JC-BP08 and triangular protrusion electrode structure has been reported [15]. It can provide optical transmittance $\sim 74\%$ at 15 V, fast average gray-to-gray (GTG) response time and manageable TFT charging issue. Thus, it is an attractive option for FSC displays.

ULH mode utilizes a rather simple homogeneous cell so that there is limited design improvement on device configuration. Thus, the ULH research mainly focuses on LC material development. From equations (8) and (10), flexoelastic coefficient e_f/K_f directly determines the on-state voltage of ULH. Enlarging flexoelastic coefficient is the most effective way to reduce operation voltage. Some bimesogenic [54–57, 60] and bent-core [58] LC materials were reported to possess a large flexoelastic coefficient. Morris *et al* [56] characterized a series of ester-linked symmetric bimesogen homologues LC materials. A relatively large flexoelastic coefficient $e_f/K_f \sim 1.74$ C/N/m of LC materials FFEnEFF was reported [56]. Recently, Varanytsia *et al* reported a giant flexoelectro-optic behavior in LC dimer CB7CB [57, 60]. The measured flexoelastic coefficient of CB7CB is 3.67 C/N/m, which can reduce the on-state voltage to ~ 11 V with a ~ 2.3 μm cell gap. We plot and fit the measured results as shown in figure 6. The agreement is quite good. However, the operation temperature of CB7CB is over 100 °C, which limits the practical applications. Merck also reported two promising ULH mixtures with operation voltages as low as 15.6 V and 19.2 V [59]. The operation temperature of Merck's ULH material ranges from <0 °C to ~ 70 °C. However, the response time (rise + decay) for the former is 5.9 ms, which is not fast enough for FSC display. In figure 6, we plot the VT curves of several materials with various flexoelastic coefficients, assuming pitch length $p \sim 300$ nm, cell gap $d \sim 3.0$ μm and small $\Delta\epsilon \sim 0$. According to figure 6, Merck's material (the one with 15.6 V) can be estimated to possess a flexoelastic coefficient $e_f/K_f \sim 3.5$ C/N/m. Further material optimization is desperately needed.

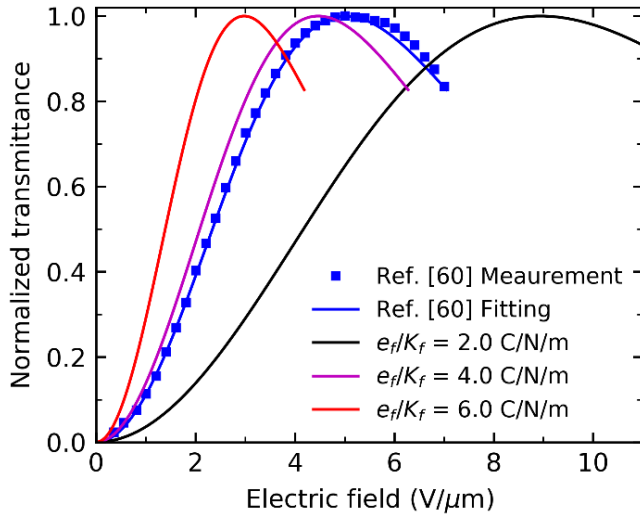


Figure 6. VT curves of ULH materials with different flexoelectric coefficients. Blue dots are measured data from [60].

So far, most of the reported USH devices with low voltage rely on dielectric effect [37, 38] rather than flexoelectric effect, because high Kerr constant material is more readily available than high flexoelectric coefficient LC material. For the USH devices based on flexoelectric effect, the operation voltage is usually over 200 V [69, 72], which is too high for practical applications. To compare the influences of these two effects, we simulate several LC materials with a typical Kerr constant $\sim 6.5 \text{ nm V}^{-2}$ or a reported highest flexoelectric coefficient $\sim 3.6 \text{ C/N/m}$. In our simulation, we used an IPS-5/5 cell with an $8.8 \mu\text{m}$ cell gap. Figure 7 shows the simulated results. Both flexoelectric effect and dielectric effect make important contributions to the EO response. To lower the operation voltage, smaller electrode gap or protruded electrode structure can be considered [38].

3.3. Response time

Fast response time of these three modes all originates from their short pitch length (p), as indicated by [38, 105, 106]:

$$\tau = \frac{\gamma}{k} \frac{p^2}{(2\pi)^2}, \quad (12)$$

where γ is the effective viscosity and k is the effective elastic constant, which are intrinsically related to the chiral dopant and the host LC material. As for the dielectric effect, γ is the rotational viscosity and k is the twist elastic constant [100, 105]. While in the flexoelectric effect, γ is the effective viscosity associated with the helix distortion [30]. According to equation (12), the response time is proportional to p^2 . In BPLC and HTN modes, CLC pitch length is typically $p \approx 300 \text{ nm}$ or less, which leads to response time in the order of $100 \mu\text{s}$ [57].

In a display panel, the majority of displayed images are in gray levels, so GTG response time is a more realistic parameter. Chen *et al* [107] investigated the GTG response of BPLC device and found that the measured GTG response time (rise and decay) keeps in sub-millisecond level. In addition, the field

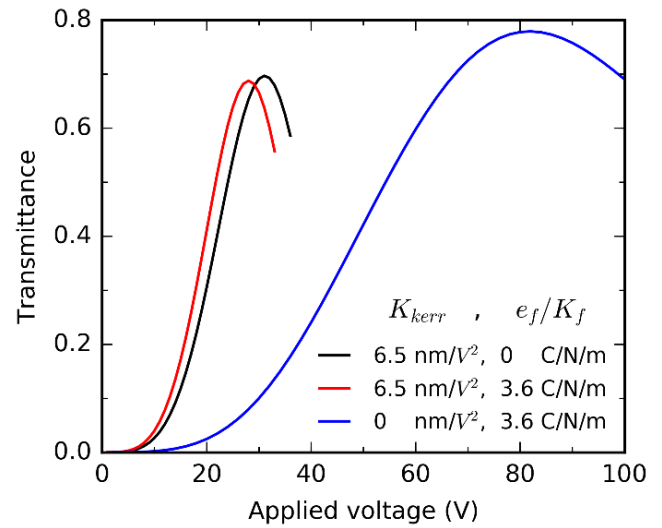


Figure 7. Simulated VT curves of USH materials with IPS 5/5 cell. Black line: pure dielectric effect. Blue line: pure flexoelectric effect. Red line: dielectric effect and flexoelectric effect co-exist.

dependent response time has been discussed in [106, 107]. The decay time of BPLC stays nearly constant for all gray levels, as indicated in equation (12). The rise time decreases as the applied voltage increases, which can be described by [106, 107]:

$$\tau_{\text{on}} = \frac{\tau_{\text{off}}}{\left(\frac{V}{V_c}\right)^2 - 1}, \quad (13)$$

where V_c is the critical voltage and τ_{off} is the decay time (equation (12)). As for flexoelectric effect, the response of helical axis rotation also follows the similar rule [34, 55]. Gou *et al* [86] measured the response time of a ULH device, and found the averaged GTG rise time is 0.35 ms and decay time is 0.53 ms . This study also indicates that rise time of ULH gets shorter while the decay time remains unchanged as the applied voltage increases.

3.4. Temperature effect

Temperature affects the physical properties, such as operation voltage and response time, of a display device. For BPLC, as equation (2) indicates, Kerr constant is determined by the birefringence Δn , dielectric anisotropy $\Delta\epsilon$ and elastic constant k of the LC host. These parameters are related to the nematic order parameter (S) as $\Delta n \sim \Delta n_0 S$ [108], $\Delta\epsilon \sim S/T$, and $k \sim S^2$ [109]. Therefore, the temperature dependent Kerr constant has the following simple form [110]:

$$K = \alpha \cdot \left(\frac{1}{T} - \frac{1}{T_c} \right), \quad (14)$$

where α is the proportionality constant. Equation (14) reveals that Kerr constant decreases as the temperature increases and vanishes at clearing point. Thus for BPLC devices, the operation voltage increases with temperature. The temperature effect of dielectric-effect-based USH mode also follows the similar rule.

While for ULH, unlike dielectric effect, the flexoelectric effect-induced helix rotation is insensitive to the temperature variation [57]. This has been confirmed by previous experiments [57, 74, 111]. Such a weak temperature effect is due to the similar temperature dependence of effective flexoelectric coefficient e_f and effective elastic constant K_f . In some bent-core [58] and bimesogenic LCs [111], the flexoelectric coefficient and elastic constant is related to temperature as $e \sim aS^2 + bS$ [112, 113] and $k \sim S^2$, respectively. Therefore, flexoelastic coefficient e_f/K_f is not sensitive to the operation temperature.

The response time of these three modes is all strongly dependent on the operation temperature. The decay time decreases rapidly as the temperature increases. Previous experimental results of BPLC [110], USH [38] and ULH modes [34, 54, 55] have clearly demonstrated this trend. As we mentioned above, elastic constant is related to order parameter as $k \sim S^2$, while the temperature dependence of viscosity γ can be expressed as [108]:

$$\gamma \sim S \cdot \exp\left(\frac{E_a}{K_B T}\right), \quad (15)$$

where E_a is the activation energy and K_B is the Boltzmann constant. Therefore, the response time in equation (12) can be rewritten as [38, 110]:

$$\tau \approx B \cdot \frac{\exp(E_a/K_B T)}{(1 - T/T_c)^\beta}, \quad (16)$$

where B is a proportionality coefficient. Equation (16) clearly explains the temperature dependence of response time.

4. CR and viewing angle

4.1. Contrast ratio (CR)

High CR is a critical requirement for display devices. The CR of a LCD is mainly governed by its dark state. As mentioned in section 2.2, the CR of ULH is still inadequate due to nonuniform alignment. The reported highest CR of ULH is only $\sim 650:1$ [73], which is much lower than that of commercial LCDs. Macroscopically, BP behaves as an optically isotropic medium (figure 3(a)). Therefore, it exhibits an excellent dark state and high CR under crossed polarizers. With regard to USH mode, its macroscopic refractive index ellipsoid is shown in figure 3(c). The optical performance of its dark state is quite similar to vertical alignment (VA) mode. As a result, USH can also provide a high CR (typically $\sim 3000:1$) [69].

When examining the CLC based modes, like BP and USH, the polarization rotation effect must be taken into consideration. Optical polarization rotation effect [114] is a common phenomenon in chiral media, like CLCs. It describes the rotation of the polarization plane of a linearly polarized light as it transmits through the LC layer. BPLC is a 3D double-twist cylinder structure, as plotted in figures 1(b) and (c). The LC molecules inside each cylinder form a symmetrical double twist structure (figures 1(d)). When a linearly polarized light

traverses these cylinders, the polarization state of the outgoing light could be rotated by a small angle. The rotated polarization leads to light leakage through the crossed polarizer and degrades the CR significantly. Liu *et al* [115] carefully investigated the polarization rotation effect in BPLCs. A small polarization rotation angle ($\sim 5^\circ$) was measured. By rotating the analyzer to compensate the polarization rotation effect, CR can be improved by $5 \times -10 \times$.

A similar polarization rotation effect also exists in USH mode, although the detailed mechanism is slightly different. Due to the random alignment of helix in BP, the incident light is not necessarily along the helical axis. Thus, only a portion of the LC would contribute to the polarization rotation effect. While for USH, the CLC helix is parallel to the incident light propagation direction, which means all the LC molecules would contribute to the polarization rotation. Accordingly, its optical rotatory power can be described by de Vries equation [36, 69, 116]:

$$\frac{\partial \Psi}{\partial z} = -\frac{2\pi}{p} \frac{(\Delta n / \bar{n})^2}{8 \left(\frac{\lambda}{\bar{n}p}\right) \left[1 - \left(\frac{\lambda}{\bar{n}p}\right)^2\right]}, \quad (17)$$

where $\Delta n = n_e - n_o$ and $\bar{n} = \sqrt{(n_e^2 + n_o^2)/2}$. According to equation (17), the optical rotatory power depends on the pitch length, birefringence, incident wavelength and propagation distance. The polarization rotation is also temperature dependent [112], since Δn decreases as temperature increases. Actually, the polarization rotation effect of USH mode has not been systematically investigated in previous publications. Here, we measured the polarization rotation angle of our USH cell at three wavelengths: $\lambda = 457$ nm, 514 nm, and 633 nm. Results are plotted in figure 8. We also fit the measured data with equation (17). Good agreement between experiment and theory is achieved. From figure 8, we find that different wavelength has a different optimal analyzer rotation angle. If we fix the analyzer at 2.4° , then the CR for the white light (60% green, 30% red and 10% blue) can be improved by about $2.5 \times$.

4.2. Viewing angle

Viewing angle is an important characteristic for a display device. Among the three modes studied, BPLC should exhibit the best viewing angle performance because it behaves like an isotropic medium at voltage-off state. Therefore, the light leakage is mainly caused by the crossed polarizers at oblique angles. However, as we discussed above, the light leakage induced by optical polarization rotation also needs to be taken into consideration when calculating the CR at different viewing angles. Liu *et al* [117] analyzed the viewing angle performance of BPLC by considering optical polarization rotation effect. Three approaches to improve the CR and widen the viewing angle have been proposed: (1) slightly rotating the analyzer; (2) using a broadband wide-view circular polarizer [118] and (3) applying a dispersive +A film. After employing compensation films, the CR of a BPLC can achieve over $100:1$ within 85° viewing cone [117].

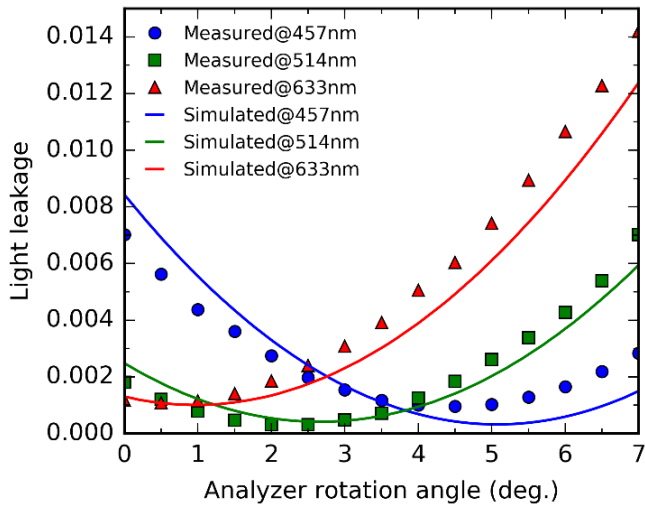


Figure 8. Measured and simulated light leakage of USH cell. Here 0° means the analyzer is crossed with polarizer.

As for ULH mode, researchers always supposed that it should exhibit a wide viewing angle due to its unique in-plane switching mechanism [81, 82, 89]. By assuming that ULH pattern can be ideally aligned, Tan *et al* [35] quantitatively demonstrated that ULH’s viewing angle characteristic is similar to that of IPS or fringe-field switching (FFS) LCD [119, 120]. Based on the simulated LC director distributions (figure 2), the isocontrast contour was calculated by applying 2×2 extended Jones matrix [98] or 4×4 Jones matrix method [99]. The simulated isocontrast contour of ULH cell is plotted in figure 9(a). Moreover, compensation films for IPS or FFS can also be adopted to widen the viewing cone of ULH due to their similarity. Both two uniaxial films (+A plate & +C plate) method and one biaxial film method work well. Figure 9(b) depicts the simulated isocontrast contour of the ULH cell compensated by one biaxial film. In comparison with uncompensated ULH (figure 9(a)), the viewing angle is greatly widened. High contrast over 300:1 within 85° viewing cone can be achieved.

The viewing angle analysis of USH mode is more complicated than BP or ULH mode for two reasons: (1) it behaves like a VA cell at voltage-off state (figure 3(c)), and (2) there exists the polarization rotation effect. That means we need to take into account these two factors at the same time. So far, there is no detailed investigation on USH’s viewing angle. Here, based on our model described in section 3.1, we are able to analyze the viewing angle of USH mode. From a practical application viewpoint, we simulate the viewing angle of dielectric effect-based USH mode because it has lower operation voltage and more mature material system than the flexoelectric effect-based USH. The parameters used in our simulation are deduced from our experiment, as described in section 3.1.

Figure 10 shows the simulated isocontrast contour of a USH cell sandwiched between two crossed polarizers after taking into consideration of the polarization rotation effect. In order to widen viewing angle, the compensation method for VA mode can also be applied [121]. The device configuration is shown in figure 11(a). The analyzer and -A film above USH cell are slightly rotated to compensate for the polarization rotation. Due to the employed compensation films, the

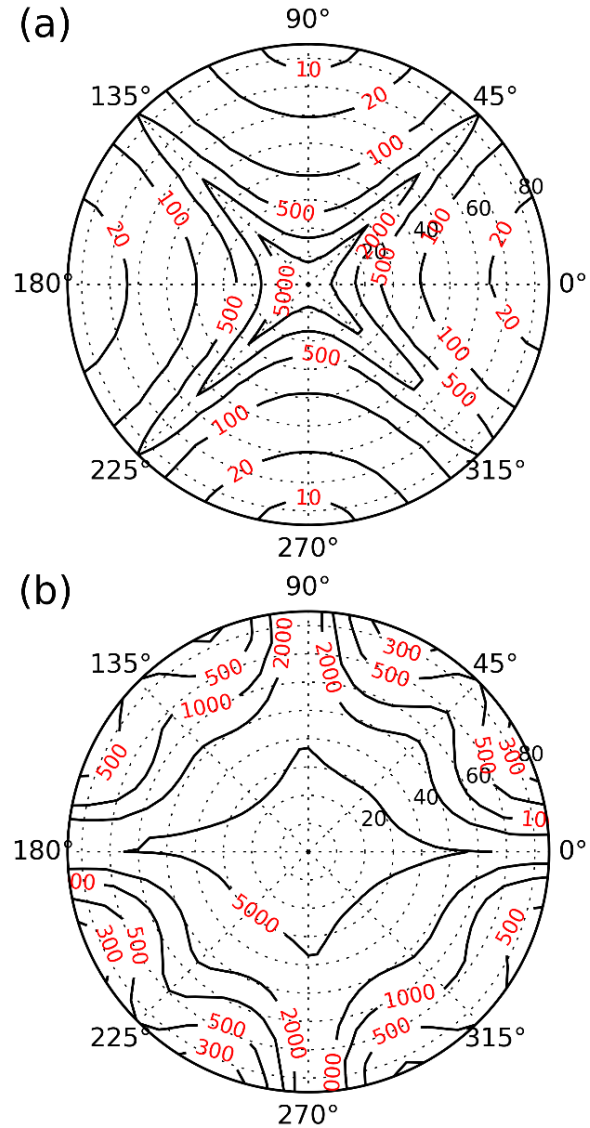


Figure 9. Simulated isocontrast contours of ULH mode: (a) uncompensated and (b) compensated with a biaxial film. Reprinted from [35], with the permission of AIP Publishing.

required rotation angle is different from the measured angle shown in figure 8. By parametric sweep, we find the optimal rotation angle is $\sim 1.8^\circ$. The compensated viewing angle is shown in figure 11(b). The viewing cone is widened to over 60° with CR > 100:1. However, the wavelength dispersion of optical rotation effect limits this method. For a different wavelength, the optimal rotation angle of analyzer varies (figure 8). In reality, the display backlight consists of RGB components, but in figure 11 we only optimize the viewing angle at $\lambda = 550$ nm. To optimize the CR for white light, we need to take into account the red and blue lights as well. Another legitimate concern is temperature effect. Since the polarization rotation depends on temperature, the optimal compensation conditions may shift as the temperature varies.

Another approach to widen the viewing cone is to employ wide-view broadband circular polarizers [118]. The advantage of using such circular polarizers is to get rid of the polarization rotation effect, because it can convert a linearly polarized incident light to a circularly polarized light. Besides, it is a

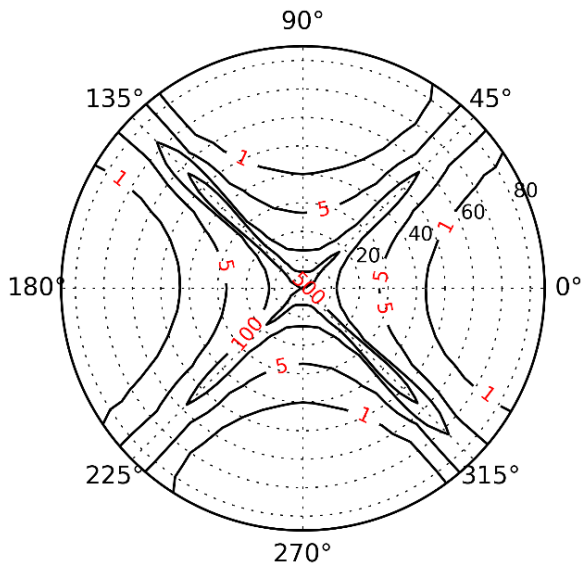


Figure 10. Simulated isocontrast contour of uncompensated USH mode at $\lambda = 550$ nm.

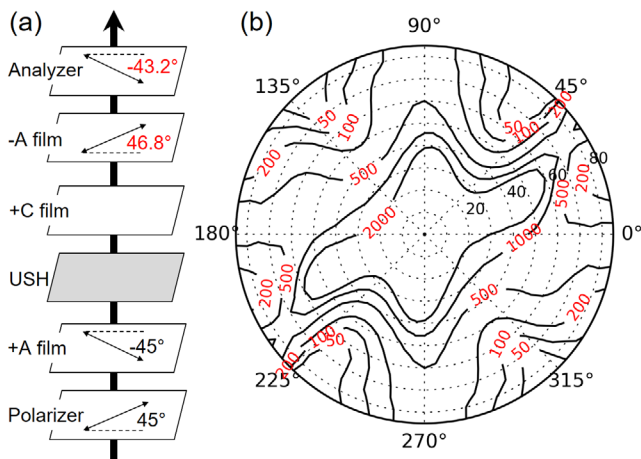


Figure 11. (a) Scheme of compensated USH device with three uniaxial films and (b) simulated isocontrast contour of compensated USH device at $\lambda = 550$ nm.

broadband polarizer, so the light leakage of RGB colors can be suppressed simultaneously. Figure 12(a) shows the phase compensation schematic. Because the USH itself works as a $-C$ film, we should use a $+C$ plate to compensate the USH cell. Moreover, to widen the viewing angle while suppressing the gamma shift, we also adopt the two-domain zigzag IPS structure for USH cell. The simulated isocontrast contour of compensated two-domain USH cell is presented in figure 12(b). $CR > 100:1$ is achieved over 85° viewing cone.

4.3. Gamma shift

In addition to isocontrast contour, gamma shift is another parameter to evaluate the angular dependence of an LCD [122]. The gamma shift of IPS-BPLC has been analyzed in previous publications [15, 123]. A single-domain BPLC would exhibit grayscale inversion. In order to suppress the grayscale inversion and widen viewing angle, a two-domain

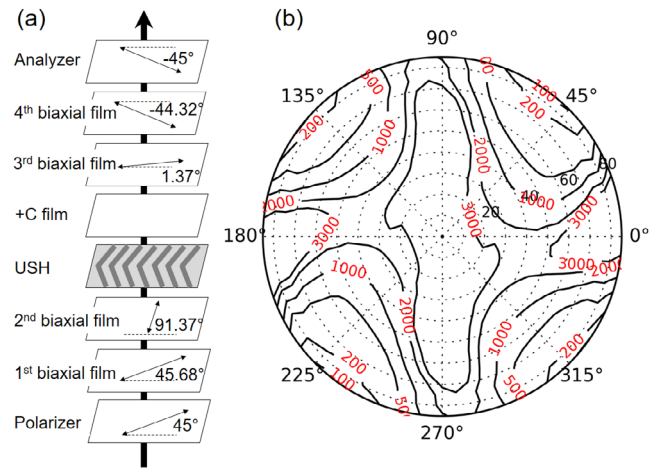


Figure 12. (a) Scheme of compensated USH device with circular polarizers and (b) simulated isocontrast contour of compensated USH device.

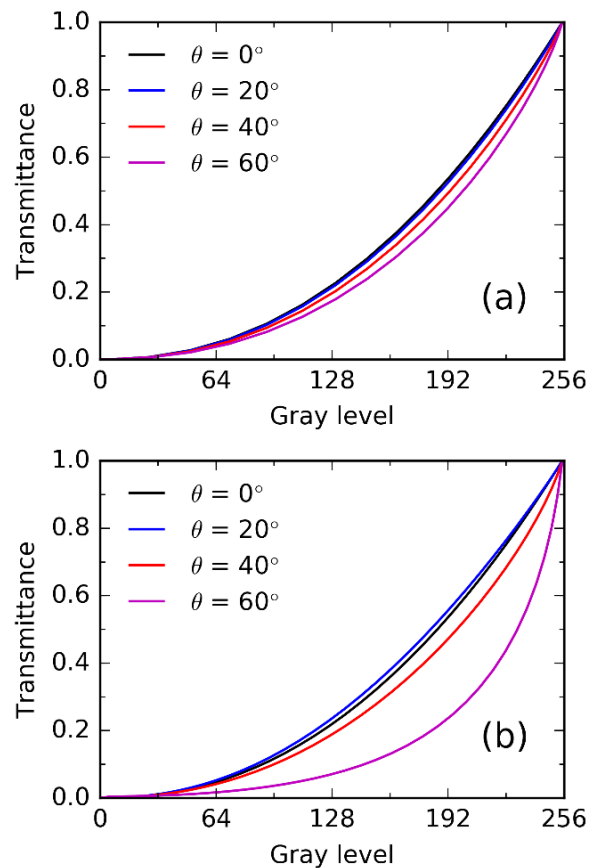


Figure 13. Simulated gamma curves at 45° azimuthal angle: (a) compensated ULH mode and (b) compensated USH mode.

zigzag structure and biaxial compensation film can be applied [123]. The compensated IPS-BPLC mode can achieve off-axis image distortion index $D < 0.2$, which means the gamma shift is unnoticeable to the human eye [15, 122].

As to ULH and USH modes, the gamma shift remains to be investigated. Here, with our proposed simulation models, we are able to calculate the gamma curves of ULH and USH modes. The gray level (GL , $G0$ - $G255$) was calculated

Table 2. Comparison between BP, USH and ULH modes.

	BP	USH	ULH
Operational voltage	~15 V with protruded electrodes [15]	>50 V with flat electrodes [37, 38]	~15 V [57, 59, 60]
Maximum transmittance	Depends on electrode configuration, normally <80% [15, 94]	Depends on electrode configuration, normally <80% [38]	Theoretically ~100% [35]
Response time	<1 ms	<1 ms	<1 ms
CR	>1000:1 [115, 117]	>3000:1 [69]	<650:1 [73]
Viewing angle	Excellent (optically isotropic dark state)	Good (VA-like dark state) [69]	Good (IPS/FFS-like dark state) [35]
Threshold-like behavior	Yes [68]	Yes	No [35]
Image flickering	No	Maybe (for flexoelectric-effect-based USH) [72]	Yes [35]
Optical polarization rotation	Yes [115]	Yes [36]	No
Alignment	Not necessary	Simple alignment procedure [38]	Complicated alignment procedure [73–88]
Charging issue	Yes [52, 53]	Maybe (for dielectric-effect-based USH)	No

from transmittance (T) by $T = (GL/255)^{2.2}$. In our simulation of gamma shift, we have considered the AC driving because flexoelectric switching depends on the electric field polarity. The ULH mode exhibits unnoticeable gamma shift within a wide viewing cone, due to its unique in-plane switching property. The gamma curves along the most severe gamma shift direction (azimuthal angle 45°) are plotted in figure 13(a). The distortion index is only $D(60^\circ, 45^\circ) = 0.177$. While for USH, gamma shift is a serious concern. The most severe gamma shift at 45° azimuthal angle is indicated in figure 13(b). The image distortion index $D(60^\circ, 45^\circ)$ reaches 1.32. One way to reduce the gamma shift of USH cell is to use more domains, similar to VA mode.

5. Discussion

Due to their submillisecond response time, BPLC, ULH and USH modes attract tremendous attention. These three modes are considered as strong candidates for next generation displays. BPLC is the most mature one among these modes and it seems ready for commercial applications [15, 51]. While for ULH and USH modes, there remains some challenges.

As for ULH mode, following technical challenges should be tackled before its prime time would arrive. The first issue is how to achieve high CR. The CR of ULH cell is critically dependent on the alignment quality. In comparison with nematic LCDs, e.g. VA (CR \approx 5000:1) for TVs and FFS (CR \approx 2000:1) for smartphones, ULH still has a long way to go. Image flickering is another important issue for flexoelectric effect-based devices. For a TFT LCD, AC voltage is used in order to avoid ionic charges accumulation. Since the flexoelectric switching is dependent on the electric field polarity, a transient image flickering occurs when the polarity of the electric field changes [72, 86]. The third issue is threshold voltage [35]. From figure 6, ULH mode does not exhibit a threshold-like behavior. When a ULH panel is addressed by active matrix, any voltage fluctuation from TFTs could cause

light leakage in the dark state and degrade the CR. So far, the ULH material system is not yet mature. New materials with large flexoelectric effect (for low voltage), low viscosity (for fast response time), wide operation temperature range, and long-term stability are desperately needed.

For USH mode, high operation voltage is the bottleneck. To lower the operation voltage to below 15 V, a large Kerr constant material and protruded electrodes offers a possible solution. However, using a high $\Delta\epsilon$ material to lower the operation voltage may cause slow capacitor charging time, similar to BPLCs. Although protrusion electrode works well for BPLC, it may not work too well for USH. This is because USH requires molecular alignment, but BPLC does not. Alignment uniformity of USH in protruded IPS electrodes needs to be examined. Another issue of USH is color shift and gamma shift, similar to a VA LCD. More efforts on developing new compensation methods and multi-domain structure are needed.

In table 2, we summarize the key performance metrics of BP, USH and ULH modes from the aspects of operation voltage, maximum transmittance, response time, CR, and viewing angle. Some potential technical challenges, such as threshold voltage, alignment, image flickering, and charging issues are also included.

6. Conclusion

We have reviewed three LC modes, namely BP, USH and ULH, with potentially submillisecond response time. Their working mechanisms, EO behaviors, response time, temperature effect, CR, and viewing angle properties are discussed. We also presented a new simulation model for analyzing USH by taking flexoelectric and dielectric effects into account simultaneously. Based on our model, the viewing angle and gamma shift of USH and ULH LCDs are investigated. Finally, we discuss some remaining challenges of these modes for practical display applications.

Acknowledgment

The authors are indebted to a.u.Vista Inc. for financial support.

ORCID iDs

Shin-Tson Wu  <https://orcid.org/0000-0002-0943-0440>

References

- [1] Schadt M 2009 *Japan. J. Appl. Phys.* **48** 03B001
- [2] Tang C W and VanSlyke S A 1987 *Appl. Phys. Lett.* **51** 913
- [3] Barnes D 2013 *SID Symp. Digest of Technical Papers* vol 44 p 26
- [4] Ukai Y 2013 *SID Symp. Digest of Technical Papers* vol 44 p 28
- [5] Peng F, Chen H and Wu S T 2017 *SID Symp. Digest of Technical Papers* vol 48 p 478
- [6] Chen H, Ha T H, Sung J H, Kim H R and Han B H 2010 *J. Soc. Inf. Dis.* **18** 57
- [7] Chen H, Zhu R, Li M C, Lee S L and Wu S T 2017 *Opt. Express* **25** 1973
- [8] Luo Z, Chen Y and Wu S T 2013 *Opt. Express* **21** 26269
- [9] Luo Z, Xu D and Wu S T 2014 *J. Disp. Technol.* **10** 526
- [10] Chen H, He J and Wu S T 2017 *IEEE J. Sel. Top. Quantum Electron.* **23** 1900611
- [11] Okuyama K *et al* 2017 *SID Symp. Digest of Technical Papers* vol 48 p 1166
- [12] Harding M J, Horne I P and Yaglioglu B 2017 *SID Symp. Digest of Technical Papers* vol 48 p 793
- [13] Peng F, Chen H, Gou F, Lee Y H, Wand M, Li M C, Lee S L and Wu S T 2017 *J. Appl. Phys.* **121** 023108
- [14] Chen C H, Lin F C, Hsu Y T, Huang Y P and Shieh H P D 2009 *J. Disp. Technol.* **5** 34
- [15] Huang Y, Chen H, Tan G, Tobata H, Yamamoto S I, Okabe E, Lan Y F, Tsai C Y and Wu S T 2017 *Opt. Mater. Express* **7** 641
- [16] Bailey R E, Arthur J J T III and Williams S P 2004 *Proc. SPIE* **5424** 99
- [17] Wu S T 1989 *Appl. Opt.* **28** 48
- [18] Chen H, Hu M, Peng F, Li J, An Z and Wu S 2015 *Opt. Mater. Express* **5** 655
- [19] Chen H, Peng F, Gou F, Lee Y H, Wand M and Wu S T 2016 *Optica* **3** 1033
- [20] Gauza S, Zhu X, Piecek W, Dabrowski R and Wu S T 2007 *J. Disp. Technol.* **3** 250
- [21] Wu S T 1990 *Appl. Phys. Lett.* **57** 986
- [22] Channin D J 1975 *Appl. Phys. Lett.* **26** 603
- [23] Channin D J and Carlson D E 1976 *Appl. Phys. Lett.* **28** 300
- [24] Kim J W, Choi T H and Yoon T H 2014 *Appl. Opt.* **53** 5856
- [25] Gou F, Chen H, Li M C, Lee S L and Wu S T 2017 *Opt. Express* **25** 7984
- [26] Srivastava A K, Chigrinov V G and Kwok H S 2015 *J. Soc. Inf. Dis.* **23** 253
- [27] Guo Q, Srivastava A K, Pozhidaev E P, Chigrinov V G and Kwok H S 2014 *Appl. Phys. Express* **7** 021701
- [28] Gerber P R 1985 *Mol. Cryst. Liq. Cryst.* **116** 197
- [29] Kikuchi H, Yokota M, Hisakado Y, Yang H and Kajiyama T 2002 *Nat. Mater.* **1** 64
- [30] Hisakado Y, Kikuchi H, Nagamura T and Kajiyama T 2005 *Adv. Mater.* **17** 96
- [31] Kikuchi H, Nagamura T and Kajiyama T 2005 *Adv. Mater.* **17** 2311
- [32] Meyer R B 1969 *Phys. Rev. Lett.* **22** 918
- [33] Patel J S and Meyer R B 1987 *Phys. Rev. Lett.* **58** 1538
- [34] Lee S D, Patel J S and Meyer R B 1990 *J. Appl. Phys.* **67** 1293
- [35] Tan G, Lee Y H, Gou F, Hu M, Lan Y F, Tsai C Y and Wu S T 2017 *J. Appl. Phys.* **121** 173102
- [36] Castles F, Morris S M and Coles H J 2009 *Phys. Rev. E* **80** 031709
- [37] Lorenz A, Gardiner D J, Morris S M, Castles F, Qasim M M, Choi S S, Kim W S, Coles H J and Wilkinson T D 2014 *Appl. Phys. Lett.* **104** 071102
- [38] Yuan J, Tan G, Xu D, Peng F, Lorenz A and Wu S T 2015 *Opt. Mater. Express* **5** 1339
- [39] Ge Z, Gauza S, Jiao M, Xianyu H and Wu S T 2009 *Appl. Phys. Lett.* **94** 101104
- [40] Yan J, Rao L, Jiao M, Li Y, Cheng H C and Wu S T 2011 *J. Mater. Chem.* **21** 7870
- [41] Chen Y and Wu S T 2014 *J. Appl. Polym. Sci.* **131** 40556
- [42] Xu D, Yuan J, Schadt M and Wu S T 2014 *Appl. Phys. Lett.* **105** 081114
- [43] Rao L, Yan J, Wu S T, Yamamoto S and Haseba Y 2011 *Appl. Phys. Lett.* **98** 081109
- [44] Chen Y, Yan J, Sun J, Wu S T, Liang X, Liu S H, Hsieh P J, Cheng K L and Shiu J W 2011 *Appl. Phys. Lett.* **99** 201105
- [45] Chen Y, Xu D, Wu S T, Yamamoto S I and Haseba Y 2013 *Appl. Phys. Lett.* **102** 141116
- [46] Peng F, Chen Y, Yuan J, Chen H, Wu S T and Haseba Y 2014 *J. Mater. Chem. C* **2** 3597
- [47] Rao L, Ge Z, Wu S T and Lee S H 2009 *Appl. Phys. Lett.* **95** 231101
- [48] Lee H, Park H J, Kwon O J, Yun S J, Park J H, Hong S and Shin S T 2011 *SID Symp. Digest of Technical Papers* vol 42 p 121
- [49] Yamamoto T *et al* 2012 *SID Symp. Digest of Technical Papers* vol 43 p 201
- [50] Tsai C Y *et al* 2015 *SID Symp. Digest of Technical Papers* vol 46 p 542
- [51] Hung C C *et al* 2017 *SID Symp. Digest of Technical Papers* vol 48 p 482
- [52] Tu C D, Lin C L, Yan J, Chen Y, Lai P O and Wu S T 2013 *J. Disp. Technol.* **9** 3
- [53] Lin C L, Tu C D, Cheng M H, Hung C C, Lin C H and Sugiura N 2015 *IEEE Electron Device Lett.* **36** 354
- [54] Musgrave B, Lehmann P and Coles H J 1999 *Liq. Cryst.* **26** 1235
- [55] Coles H J, Clarke M J, Morris S M, Broughton B J and Blatch A E 2006 *J. Appl. Phys.* **99** 034104
- [56] Morris S M, Clarke M J, Blatch A E and Coles H J 2007 *Phys. Rev. E* **75** 041701
- [57] Varanytsia A and Chien L C 2016 *J. Appl. Phys.* **119** 014502
- [58] Balachandran R, Panov V P, Vij J K, Lehmann A and Tschierske C 2013 *Phys. Rev. E* **88** 032503
- [59] Siemianowski S, Bremer M, Plummer E, Fiebranz B, Klasen-Memmer M and Canisius J 2016 *SID Symp. Digest of Technical Papers* vol 47 p 175
- [60] Varanytsia A and Chien L C 2017 *Sci. Rep.* **7** 41333
- [61] Meiboom S and Sammon M 1980 *Phys. Rev. Lett.* **44** 882
- [62] Cheng H C, Yan J, Ishinabe T and Wu S T 2011 *Appl. Phys. Lett.* **98** 261102
- [63] Cheng H C, Yan J, Ishinabe T, Sugiura N, Liu C Y, Huang T H, Tsai C Y, Lin C H and Wu S T 2012 *J. Disp. Technol.* **8** 98
- [64] Cheng H C, Yan J, Ishinabe T, Lin C H, Liu K H and Wu S T 2012 *J. Disp. Technol.* **8** 627
- [65] Yan J and Wu S T 2011 *Opt. Mater. Express* **1** 1527
- [66] Joshi P *et al* 2015 *Appl. Phys. Lett.* **106** 101105
- [67] Yan J, Chen Y, Wu S T and Song X 2013 *J. Disp. Technol.* **9** 24
- [68] Yan J and Wu S T 2011 *J. Disp. Technol.* **7** 490
- [69] Castles F, Morris S M, Gardiner D J, Malik Q M and Coles H J 2010 *J. Soc. Inf. Dis.* **18** 128

- [70] Gardiner D J, Morris S M, Castles F, Qasim M M, Kim W S, Choi S S, Park H J, Chung I J and Coles H J 2011 *Appl. Phys. Lett.* **98** 263508
- [71] Broughton B J, Clarke M J, Blatch A E and Coles H J 2005 *J. Appl. Phys.* **98** 034109
- [72] Joshi V, Chang K H, Paterson D A, Storey J, Imrie C T and Chien L C 2017 *SID Symp. Digest of Technical Papers* vol 48 p 1849
- [73] Salter P, Elston S J, Raynes P and Parry-Jones L A 2009 *Japan. J. Appl. Phys.* **48** 101302
- [74] Rudquist P, Komitov L and Lagerwall S T 1998 *Liq. Cryst.* **24** 329
- [75] Inoue Y and Moritake H 2015 *Appl. Phys. Express* **8** 071701
- [76] Inoue Y and Moritake H 2015 *Appl. Phys. Express* **8** 061701
- [77] Komitov L, Bryan-Brown G P, Wood E L and Smout A B J 1999 *J. Appl. Phys.* **86** 3508
- [78] Carbone G, Salter P, Elston S J, Raynes P, De Sio L, Ferjani S, Strangi G, Umetsu C and Bartolino R 2009 *Appl. Phys. Lett.* **95** 011102
- [79] Hegde G and Komitov L 2010 *Appl. Phys. Lett.* **96** 113503
- [80] Carbone G, Corbett D, Elston S J, Raynes P, Jesacher A, Simmonds R and Booth M 2011 *Mol. Cryst. Liq. Cryst.* **544** 37
- [81] Outram B I and Elston S J 2013 *J. Appl. Phys.* **113** 043103
- [82] Outram B I, Elston S J, Tuffin R, Siemianowski S and Snow B 2013 *J. Appl. Phys.* **113** 213111
- [83] Wang C T, Wang W Y and Lin T H 2011 *Appl. Phys. Lett.* **99** 041108
- [84] Nian Y L, Wu P C and Lee W 2016 *Photonics Res.* **4** 227
- [85] Coles H J, Musgrave B, Coles M J and Willmott J 2001 *J. Mater. Chem.* **11** 2709
- [86] Gou F, Lee Y H, Tan G, Hu M, Lan Y F, Tsai C Y and Wu S T 2017 *SID Symp. Digest of Technical Papers* vol 48 p 1822
- [87] Gardiner D J, Morris S M, Hands P J W, Castles F, Qasim M M, Kim W S, Choi S S, Wilkinson T D and Coles H J 2012 *Appl. Phys. Lett.* **100** 063501
- [88] Kimura M and Endo N 2016 *IEICE Trans. Electron.* **99** 1240
- [89] Broughton B J, Clarke M J, Morris S M, Blatch A E and Coles H J 2006 *J. Appl. Phys.* **99** 023511
- [90] Kim S H, Chien L C and Komitov L 2005 *Appl. Phys. Lett.* **86** 161118
- [91] Kim S H, Shi L and Chien L C 2009 *J. Phys. D: Appl. Phys.* **42** 195102
- [92] Hubert P, Jägelmalm P, Oldano C and Rajteri M 1998 *Phys. Rev. E* **58** 3264
- [93] Yan J, Cheng H C, Gauza S, Li Y, Jiao M, Rao L and Wu S T 2010 *Appl. Phys. Lett.* **96** 071105
- [94] Xu D, Chen Y, Liu Y and Wu S T 2013 *Opt. Express* **21** 24721
- [95] Corbett D R and Elston S J 2011 *Phys. Rev. E* **84** 041706
- [96] Elston S J 2008 *Phys. Rev. E* **78** 011701
- [97] Rudquist P, Komitov L and Lagerwall S T 1994 *Phys. Rev. E* **50** 4735
- [98] A. Lien 1990 *Appl. Phys. Lett.* **57** 2767
- [99] Huang Y, Wu T X and Wu S T 2003 *J. Appl. Phys.* **93** 2490
- [100] Rahman M A, Said S M and Balamurugan S 2015 *Sci. Technol. Adv. Mater.* **16** 033501
- [101] Wittek M, Tanaka N, Wilkes D, Bremer M, Pauluth D, Canisius J, Yeh A, Yan R, Skjonnemand K and Klasen-Memmer M 2012 *SID Symp. Digest of Technical Papers* vol 43 p 25
- [102] Haseba Y, Yamamoto S I, Sago K, Takata A and Tobata H 2013 *SID Symp. Digest of Technical Papers* vol 44 p 254
- [103] Jiao M, Li Y and Wu S T 2010 *Appl. Phys. Lett.* **96** 011102
- [104] Chen Y, Sun Y and Yang G 2011 *Liq. Cryst.* **38** 555
- [105] Patel J S and Lee S D 1989 *J. Appl. Phys.* **66** 1879
- [106] Gleeson H F and Coles H J 1989 *Liq. Cryst.* **5** 917
- [107] Chen K M, Gauza S, Xianyu H and Wu S T 2010 *J. Disp. Technol.* **6** 49
- [108] Wu S T 1986 *Phys. Rev. A* **33** 1270
- [109] Maier W and Saupe A 1960 *Z. Naturforsch. A* **15** 287
- [110] Rao L, Yan J and Wu S T 2010 *J. Soc. Inf. Disp.* **18** 954
- [111] Noot C, Coles M J, Musgrave B, Perkins S P and Coles H J 2001 *Mol. Cryst. Liq. Cryst.* **366** 725
- [112] Osipov M A 1984 *J. Phys. Lett.* **45** 823
- [113] Cheung D L, Clark S J and Wilson M R J 2004 *J. Chem. Phys.* **123** 9131
- [114] Bensimon D, Domany E and Shtrikman S 1983 *Phys. Rev. A* **28** 427
- [115] Liu Y, Lan Y F, Zhang H, Zhu R, Xu D, Tsai C Y, Lu J K, Sugiura N, Lin Y C and Wu S T 2013 *Appl. Phys. Lett.* **102** 131102
- [116] De Vries H 1951 *Acta Cryst.* **4** 219
- [117] Liu Y, Lan Y F, Hong Q and Wu S T 2014 *J. Disp. Technol.* **10** 3
- [118] Hong Q, Wu T X, Lu R and Wu S T 2005 *Opt. Express* **13** 10777
- [119] Lee S H, Lee S L and Kim H Y 1998 *Appl. Phys. Lett.* **73** 2881
- [120] Saitoh Y, Kimura S, Kusafuka K and Shimizu H 1998 *Japan. J. Appl. Phys.* **37** 4822
- [121] Zhu X, Ge Z and Wu S T 2006 *J. Disp. Technol.* **2** 2
- [122] Kim S S, Berkeley B H, Kim K H and Song J K 2004 *J. Soc. Inf. Disp.* **12** 353
- [123] Rao L, Ge Z and Wu S T 2010 *J. Disp. Technol.* **6** 115